Effect of Dislocations on the Zero-Bias Resistance-Area Product, Quantum Efficiency, and Spectral Response of LWIR HgCdTe Photovoltaic Detectors

Vishnu Gopal and Sudha Gupta

***Abstract*—The effect of dislocations on the zero-bias resistance-area product, quantum efficiency, and spectral response of long wavelength infrared (LWIR) HgCdTe photodiodes has been modeled for a case in which the line dislocations are along the thickness of the wafer. The model focuses on the calculation of the impedance of individual dislocation followed by the calculation of the resultant effect by assuming the dislocations to be uniformly distributed in the sample. In the process, we have also obtained a new relation for estimating effective diffusion length of minority carriers as a function of dislocation density in the sample. The proposed model has been shown to provide an excellent fit to the experimental data.**

***Index Terms*—Dislocations, HgCdTe photovoltaic detectors, quantum efficiency, R_0A product, spectral response.**

I. Introduction

KNOWLEDGE of the effect of dislocations on the electrical and optical performance of HgCdTe photodiodes is an important aspect of the current as well as future HgCdTe IR detector technology as the considerable research and development effort is now directed toward fabricating large area arrays on epilayers grown on alternate substrates like Si and GaAs. Due to large mismatch of lattice constants of HgCdTe and Si–GaAs, the HgCdTe epilayers grown on these alternate substrates have a higher dislocation density than grown on high-quality lattice matched CdZnTe substrates[1], [2]. A model which could reasonably correlate the dependence of both electrical and optical performances of the photodiodes on the dislocation density of the substrate is thus desirable. Two of the models [3], [4] which have been published in the past meet the requirement only partially. Johnson *et al.* [3] proposed a phenomenological model to describe the variation of the zero-bias resistance-area product (R_0A) of their diodes with the dislocation density. Their model envisages two types of dislocations: individual dislocation and interacting dislocations. The conductance of each type of dislocation was determined by fitting the model to the experimental data under the assumption that the conductance of the junction is just the sum of the conductances of the dislocation-free junction, individual dislocations, and interacting dislocations. Their model, though matched the temperature dependence of R_0A product well however, did not describe the optical performance (quantum efficiency and spectral response) satisfactorily. In another model proposed by Jowikowski and Rogalski [4] dislocations were envisaged as cylindrical regions confined by surfaces with definite surface recombination. Both radius of dislocations and its surface recombination velocity were determined by comparison of theory with the carrier life time experimental data from the published literature. Diode performance parameters, i.e., R_0A product and quantum efficiency as a function of dislocation density were numerically computed using Van Roosbroeck model. The computed R_0A product and quantum efficiency from this model have been shown in broad agreement with the trend of the experimental data, but the gap in case of temperature dependence of R_0A product and as well as numerical nature of the model leaves the scope for proposing an alternative model. In the present paper, we are attempting to present a very simple analytical model, which begins with the computation of shunt impedance of individual dislocation using well-known concepts from the published literature.

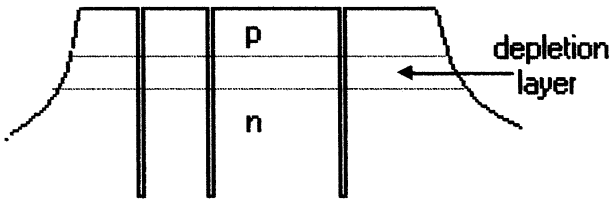

Fig. 1. Schematic of a p-on-n mesa diode showing dislocations intersecting the junction.

II. Model

Similar to the earlier models [3], [4], the model presented here visualise the dislocation lines to be running along the thickness of the sample. In other words, epilayers grown on Si–GaAs substrate are envisaged to have the dislocation lines perpendicular to the epilayer – substrate interface. When a junction is formed in such a material, these dislocations are likely to intersect the junction as shown in Fig. 1 and thus influence the junction impedance. In this paper, we will essentially attempt to first calculate the impedance of individual dislocations followed by the study of their effect on electrical and optical performances of the photodiode by assuming the dislocations to be uniformly

Manuscript received November 4, 2002; revised February 11, 2003. The review of this paper was arranged by Editor P. Bhattacharya.

The authors are with the Solid State Physics Laboratory, Timarpur, Delhi 110054 India (e-mail: VISHNU_GOPAL/sspl@ssplnet.org).

Digital Object Identifier 10.1109/TED.2003.813230

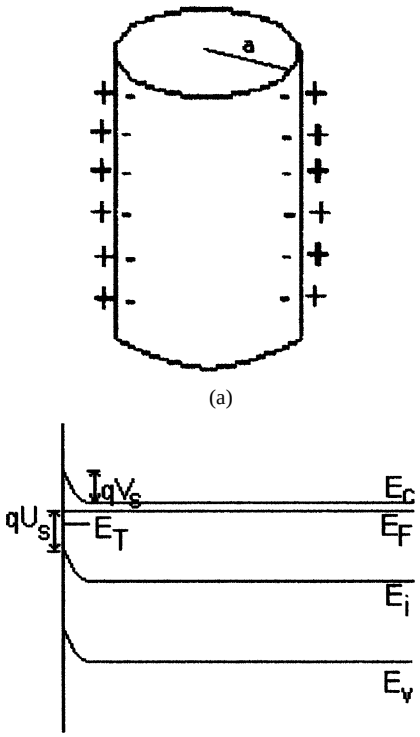

(a)

(b)

Fig. 2. (a) Schematic picture of a dislocation in the base material and (b) the energy band diagram at the material-dislocation interface.

distributed in the material. The main proposed features of the model are outlined here.

1) The regions of dislocations in the material are the regions of high recombination and that the impedance (R_s) of an individual dislocation is related to the dislocation recombination current by the following relation

$$R_S = \frac{kT}{qI_R} \tag{1}$$

where k is the Boltzmann constant, q is the fundamental charge of an electron, T is the temperature of the sample, and I_R is the dislocation recombination current.

2) Each dislocation may be viewed as a cylinder with radius equal to an integral multiple of lattice constant. The minimum value of the multiplier is assumed unity as shown in Fig. 2(a).

3) The cylindrical core of each dislocation is surrounded by space charges $Q_{\rm SC}$, leading to the formation of a depletion layer around the core and the dislocation recombination current I_R is given by

$$I_R = qn_i sA_s \tag{2}$$

where n_i is the intrinsic carrier concentration, s is the recombination velocity, and A_s is the surface area of the dislocation contributing to the recombination current.

4) Dislocation cylinders are the regions of discontinuity in the lattice and that the surface of the core of the dislocation cylinder may be treated equivalent to a clean surface in vacuum, meaning thereby that the density of surface states (N_t) is in the range of 10^{14}–10^{15} cm^{-2}.

Further, the discontinuity of the lattice at dislocations give rise to a series of levels within the bandgap of the material. However, those energy levels which significantly contribute to the recombination current are assumed to be distributed in a narrow range of energy and for the sake of simplicity, may be approximated to a single level located at an energy level E_t as shown in Fig. 2(b).

5) By treating discontinuity in the lattice at each dislocation equivalent to the discontinuity of the lattice at a planar surface, the magnitude of the recombination velocity s may be estimated in a way similar to the calculation of the recombination velocity at the surface of a semiconductor wafer. Thus it is proposed to use the following expression [5] to calculate the recombination velocity at each dislocation

$$s = \frac{\sqrt{K_n K_p}N_t(n_b + p_b)}{2n_i\left\{\cosh\left[\frac{(E_t - E_i)}{kT} - u_0\right] + \cosh\left(\frac{qU_S}{kT} - u_0\right)\right\}} \tag{3}$$

where K_n and K_p are the capture probabilities for electrons and holes, respectively, by the surface states. n_b and p_b are the electron and hole densities in the bulk, away from the dislocations. E_i is the intrinsic Fermi level in the bulk and u_0 is defined as

$$u_0 = \ln\sqrt{\frac{K_p}{K_n}}. \tag{4}$$

The potential U_s at the surface of the core of the dislocation can be determined by the combination of following equations

$$Q_{\rm SC} = q(n_b + p_b)L_{db}F_t \tag{5}$$

$$F_t = \sqrt{2}\left\{\frac{\cosh(u_b + v_s)}{\cosh u_b} - v_s\tanh u_b - 1 + \frac{N_t^*}{n_b + p_b} \cdot \left[\ln\left(1 + \frac{\exp(v_s) - 1}{1 + \exp\left(\frac{E_t}{kT}\right)}\right) - \frac{v_s}{1 + \exp\left(\frac{E_t}{kT}\right)}\right]\right\}. \tag{6}$$

N_t^* is the trap density in the space charge region. In the absence of any knowledge about the value of N_t^*, it is assumed that the strain field generated at the discontinuity causes approximately the same number of trap levels within the space region. The value of N_t^*, hence, has been taken to be numerically equal to the value of density of surface states, i.e., $N_t^* = 10^{15}$ cm^{-3}. u_s and v_s are the reduced potentials defined by

$$u_s = \frac{qU_s}{kT}$$
$$v_s = \frac{q(U_s - U_b)}{kT.} \tag{7}$$

U_b is the potential in the bulk of the material and the effective Debye length L_{db} is given by

$$L_{db} = \sqrt{\frac{\varepsilon\varepsilon_s kT}{q^2(n_b + p_b)}}. \tag{8}$$

Thus, a combination of (2) to (8) can be used to estimate impedance of an individual dislocation from (1). While applying the present model to the experimental

data, $Q_{\rm SC}$ will be treated as the variable fitting parameter.

Having stated our approach to calculate the impedance of individual dislocations, the calculation of the resultant zero bias junction impedance is straight forward since the impedance of dislocations and the junction impedance can be added in parallel, i.e.

$$\frac{1}{R_0} = \frac{1}{R_D} + \frac{NA_j}{R_S}. \tag{9}$$

Where N is the number of dislocations per unit area in the base material, A_j is the planar junction area, and R_D is the zero bias impedance of the dislocation free junction.

A. Calculation of Zero Bias Impedance

As an example we chose here p^+–n configuration of an $Hg_{1-x}Cd_xTe$ diode to discuss the present model. The dark current mechanisms dominant at zero bias for temperatures greater than 40 K are the thermal diffusion of minority carriers from quasi neutral regions, g-r current in the depletion region, and an ohmic component due to the presence of dislocations in the material. So the first term R_D in the right-hand side (RHS) of (9) includes diffusion and g-r contributions of minority carriers while the second term is the contribution of the shunt impedance. The relevant expressions used for these calculations are summarized here.

1) In a one-sided step junction, the thermal diffusion of minority carriers from the heavily doped side may be assumed negligible. The diffusion contribution to the impedance of a p^+–n junction can therefore be described by [6]

$$R_{diff0}^{-1} = \frac{q^2}{kT}\frac{n_i^2}{N_d}\frac{D_h}{L_h}A_j\frac{S_r\tau_h\cosh\left(\frac{t}{L_h}\right)+L_h\sinh\left(\frac{t}{L_h}\right)}{S_r\tau_h\sinh\left(\frac{t}{L_h}\right)+L_h\cosh\left(\frac{t}{L_h}\right)}. \tag{10}$$

where D_h and τ_h are, respectively, the diffusion constant and lifetime of the minority carriers. S_r is the surface recombination velocity at the epi-substrate interface, t is the thickness, and N_d is the concentration of the donors in the base n-layer. In case of fully ionised donors, N_d will be equal to n_b.

2) In its simplified form, g-r current contribution to the zero bias diode impedance is given by [6]

$$R_{gr0}^{-1} = \frac{q^2 n_i W_{\rm dep} A_j}{2kT\tau_{gr}}. \tag{11}$$

where $W_{\rm dep}$ is the depletion layer width and τ_{gr} is the gr lifetime of the minority carriers.

Component, R_D, of the zero bias impedance is obtained by adding (10) and (11)

$$\frac{1}{R_D} = \frac{1}{R_{dff0}} + \frac{1}{R_{gr0}}. \tag{12}$$

A detailed analysis of dark I-V characteristics and zero bias impedance of a diode in the presence of other components like trap-assisted tunnelling, band-to-band tunnelling and avalanche multiplication, etc. have been previously published [7], [8]. But in the present paper, it is sufficient to take into account only diffusion and g-r currents as already stated.

3) From (1) and (2), the impedance of an individual dislocation is

$$R_S^{-1} = \frac{q^2 n_i s A_S}{kT} \tag{13}$$

where area A_s is given by

$$A_s = 2\pi mat. \tag{14}$$

Here, a is the lattice constant of the epi material and m is the integral multiple whose value is taken as one in the present calculations.

B. Calculation of Quantum Efficiency and Spectral Response

The quantum efficiency of a backside illuminated diode is given by [9]

$$\eta = \frac{\alpha L_h}{\alpha^2 L_h^2 - 1}\left\{\left[\frac{S_r + \left(\frac{L_h^2\alpha}{\tau_h}\right)\sec h\left(\frac{t}{L_h}\right)}{S_r\tanh\left(\frac{t}{L_h}\right)+\frac{L_h}{\tau_h}}\right] - [\alpha L_h\exp(-\alpha t)] - \left[\frac{\left(\frac{L_h}{\tau_h}\right)\tanh\left(\frac{t}{L_h}\right)+S_r}{S_r\tanh\left(\frac{t}{L_h}\right)+\frac{L_h}{\tau_h}}\exp(-\alpha t)\right]\right\} \tag{15}$$

where α is the optical absorption coefficient of the material.

It is clear from the above expression that the effect of dislocations on the quantum efficiency will be manifested through the effect of dislocations on the diffusion length of illumination induced minority carriers in the base of the diode. Equation (9) provides us a basis for calculating the effect of dislocations (due to recombination of carriers) on the minority carrier diffusion length. Effect of dislocations on minority carrier mobility, if any, will be assumed negligible. Omitting the contribution of g-r mechanism, as it has no effect on minority carrier diffusion length in the base region of the diode, (9) may be rewritten as follows:

$$\frac{1}{R_0} = \frac{1}{R_{diff0}} + \frac{NA_j}{R_S}. \tag{16}$$

After taking in to account the minority carriers generated on illumination and substituting the values of R_{diff0} and R_s from (10) and (13), (16) can be rewritten as

$$\begin{aligned}&\frac{q^2}{kT}\left(\frac{n_i^2}{N_d}+\Delta p\right)\frac{D_h}{L_{\rm eff}}A_j \frac{S_r\tau_{\rm eff}\cosh\left(\frac{t}{L_{\rm eff}}\right)+L_{\rm eff}\sinh\left(\frac{t}{L_{\rm eff}}\right)}{S_r\tau_{\rm eff}\sinh\left(\frac{t}{L_{\rm eff}}\right)+L_{\rm eff}\cosh\left(\frac{t}{L_{\rm eff}}\right)}\\ &=\frac{q^2}{kT}\left(\frac{n_i^2}{N_d}+\Delta p\right)\frac{D_h}{L_h}A_j\frac{S_r\tau_h\cosh\left(\frac{t}{L_h}\right)+L_h\sinh\left(\frac{t}{L_h}\right)}{S_r\tau_h\sinh\left(\frac{t}{L_h}\right)+L_h\cosh\left(\frac{t}{L_h}\right)} + \frac{q^2}{kT}(n_i+\Delta p)\frac{sA_SN}{kT}A_j\end{aligned} \tag{17}$$

where Δp is the minority carrier concentration generated in the material on illumination. In general, $\Delta p \gg n_i^2/N_d$ or n_i. Hence (17) gets simplified to the following form:

$$\frac{1}{L_{\text{eff}}}\frac{S_r\tau_{\text{eff}}\cosh\left(\frac{t}{L_{\text{eff}}}\right)+L_{\text{eff}}\sinh\left(\frac{t}{L_{\text{eff}}}\right)}{S_r\tau_{\text{eff}}\sinh\left(\frac{t}{L_{\text{eff}}}\right)+L_{\text{eff}}\cosh\left(\frac{t}{L_{\text{eff}}}\right)} = \frac{1}{L_h}\frac{S_r\tau_h\cosh\left(\frac{t}{L_h}\right)+L_h\sinh\left(\frac{t}{L_h}\right)}{S_r\tau_h\sinh\left(\frac{t}{L_h}\right)+L_h\cosh\left(\frac{t}{L_h}\right)}+\frac{sA_SN}{D_h}. \quad (18)$$

Calculation of L_{eff} is not straightforward from the above equation because of the involvement of hyperbolic functions on the left-hand side (LHS). It is however possible to further simplify (18) to a simpler form by assuming: $t \ll L_h$ and L_{eff}, and $S_r \to 0$

$$\frac{1}{L_{\text{eff}}^2} = \frac{1}{L_h^2}+\frac{2\pi masN}{D_h}. \quad (19)$$

Note that (19) closely resembles to the relation used previously by some authors [3], [4], [10]–[12] for estimating the effect of dislocation density on the diffusion length. In the present paper, we will show that the estimates of effective diffusion length of minority carriers obtained from (19) match the experimental data on quantum efficiency and spectral response of the HgCdTe photodiodes much better than obtained by using previously reported relation.

III. Results and Discussion

In this section, we will test the model described earlier against the experimental data reported by Johnson *et al.* [3]. Their work was essentially carried out to study the effect of dislocations on the electrical and optical properties of HgCdTe photovoltaic detectors by intentionally indenting localized regions of high performance LWIR HgCdTe arrays of p-on-n double-layer-heterojunction (DLHJ) backside illuminated detectors. As will be seen later the detailed data reported in this paper has enabled us to test the present model for the variation of R_0A product as a function of dislocation density, variation in R_0A as a function of temperature in diodes with high dislocation density, variation in the quantum efficiency of photodiodes as a function of dislocation density and the variations in spectral response as a function of dislocation density. The use of Johnson *et al.*'s data to test the present model may be justified on the assumption that the properties of the DLHJ photodiodes are mainly governed by the contribution from the lightly doped narrow gap n-type base layer and that the contribution from the high-doped wider gap p-type cap layer is negligible.

A. Dislocation Dependence of R_0A

To be able to apply the present model to the experimental data of Johnson *et al.* [3] it is proposed to first fit the homojunction model to the experimental data (squares in Fig. 3) on the temperature dependence of R_0A product on diodes fabricated in good quality material before indentation. As shown in Fig. 3 fitting of the theory (continuous line) with the experiment has been carried out in the higher temperature region as the contribution from trap-assisted tunnelling cannot be ignored at temperatures

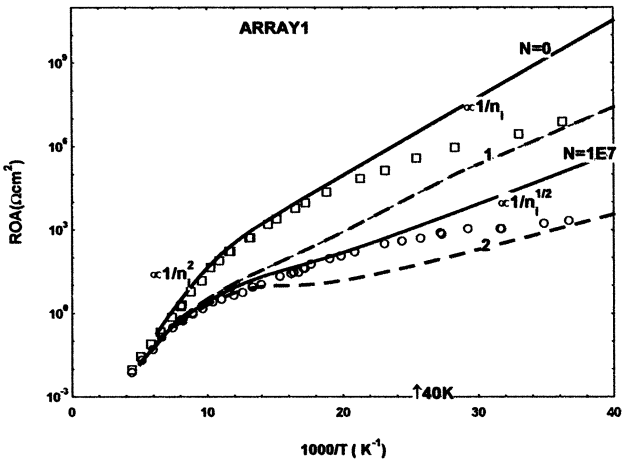

Fig. 3. Temperature variation of R_0A of diodes with 9.5-μm cutoff wavelength. Continuous line curves are the calculated curves using the present model in the absence of dislocations ($N = 0$) and for high dislocation density ($N = 10^7$ cm^{-2}) with space charge density 5.4×10^{10} cm^{-2}. Broken line curves marked 1 and 2 are the calculated curves for high dislocation density using present model with space charge density of 5.0×10^{10} cm^{-2} and 5.8×10^{10} cm^{-2}, respectively, while points are the experimental data from [3].

TABLE I
Material Parameters Used for Dark Current Calculations

Parameter	Symbol	Value	Reference
Minority carrier lifetime	τ_h	2.5μ sec	By fitting
Minority carrier mobility	μ_h	500 cm^2 V^{-1}sec^{-1}	By fitting
electron concentration in n-region	N_d (fully ionised donors)	1x10^{15}cm^{-3}	13,14
Hole concentration in p$^+$-region	N_a	1.7x10^{17}cm^{-3}	13,14,15
Trap energy level	E_t	1.4 E_i	15
Capture cross-section for holes	K_p	1x10^{-8}cm^{3}sec^{-1}at 77K	15
Capture cross-section for electrons	K_n	9x10^{-10}cm^{3}sec^{-1} at 77K	15
Surface state density	N_t	1x10^{15}cm^{-2}	5
space charge density	Q_{ss}/q	5.4x10^{10}cm^{-2} (array1) 5.2x10^{10}cm^{-2} (array2)	By fitting
Lattice constant of the base material.	a	6.4x10^{-8}cm	16

below 40 K. In the present model the contribution of the latter has been omitted. Some of the material parameters that are not mentioned in [3] but have been now obtained either by fitting or taken from the literature [13]–[16] are summarized in Table I and will be used in the subsequent calculations. The temperature dependence of the band gap and intrinsic carrier concentration is taken in to account by using widely used formulas from [17] and [18], respectively.

Fig. 3 also shows the comparison of the present model (continuous line curve) with the experimental data (circles) in case of diodes with dislocation density of 10^7 cm^{-2}. It can be seen that the present model follow the experimental data well for a space charge density of 5.4×10^{10} cm^{-2} around the core of the dislocations. The additional two broken lines marked 1 and 2, respectively, corresponds to the space charge densities of 5.8×10^{10} and 5×10^{10} cm^{-2} and have been shown here to emphasise the sensitiveness of shunt impedance of the dislocations on the magnitude of space charge around the core. Obviously the domi-

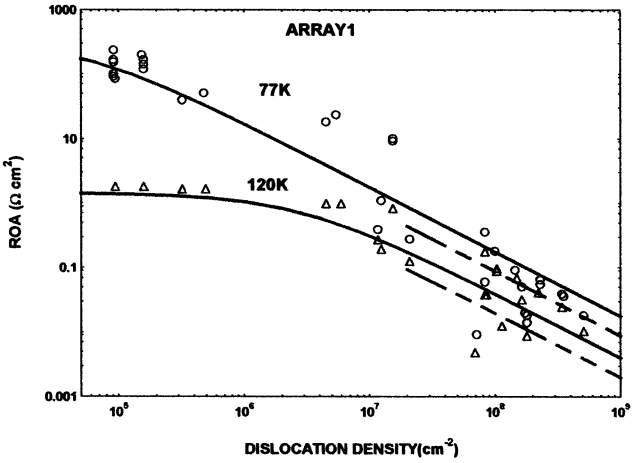

Fig. 4. Variation of R_0A versus dislocation density in the base material for diodes with 9.5-μm cutoff wavelength (array 1) at two temperatures (77 and 120 K). Continuous and broken lines are respectively calculated curves using the present model for $m = 1$ and 2 (meaning thereby the dislocation cylinders of radius equal to one and two lattice constants) while points are the experimental data taken from [3].

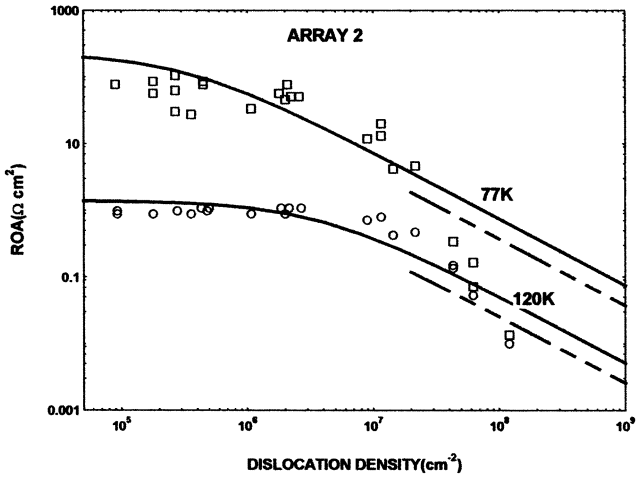

Fig. 5. Variation of R_0A versus dislocation density in the base material for diodes with 10.3-μm cutoff wavelength (array 2) at two temperatures (77 and 120 K). Continuous and broken lines are, respectively, calculated curves using the present model for $m = 1$ and 2 (meaning thereby the dislocation cylinders of radius equal to one and two lattice constants) while points are the experimental data taken from [3].

nance of shunt impedance is responsible for the variations in R_0A in this region. Physically, the rate of recombination of minority carriers (holes in this case) depends on the effectiveness of surface states in capturing both holes and electrons. For depletion layer in n-type material, the rate limiting process is the capture of electrons by these states because even though the states are vacant, very few electrons are able to reach the dislocation surface states. As the space charge increases, this number becomes even smaller. This leads to the reduction in the rate of recombination and hence the variations in R_0A product in the shunt dominated region. Based on the present example we are encouraged to suggest that the observed temperature dependence of R_0A proportional to $1/n_i^{1/2}$ may be interpreted due to the dominating contribution from the shunt impedance of dislocations in the wafer.

Next, Figs. 4 and 5 show the calculated dependence of R_0A product as a function of dislocation density for two $Hg_{1-x}Cd_xTe$ arrays of cutoff wavelengths 9.5 μm and 10.3 μm at 77 K and 120 K. It is seen that the present model (continuous line) fits very well with the experimental data points up to the dislocation densities of 10^7 cm^{-2}. The model, however, deviates from the experimental data in the higher dislocation density range possibly due to neglecting of the contribution of "interacting" dislocations [3]. Note that this model considers only one type of dislocations namely individual dislocations. Another possible alternative explanation for the observed deviation between the present model and the experimental data could be the merger of few dislocations leading to the larger surface area of some of the dislocation cylinders or clustering of dislocations in the range of higher dislocation densities. Broken line curves in Figs. 4 and 5 show the degradation in R_0A product if the radius of the dislocation cylinder was two lattice constants rather than only one lattice constant. Alternatively this would also mean double the dislocation density due to clustering. The large scatter of the experimental data at high dislocation densities may be then interpreted as a possible indication of the variations in the size of the dislocations due to the variations in the number of dislocations merging together at different sites or clustering of dislocations within a given wafer.

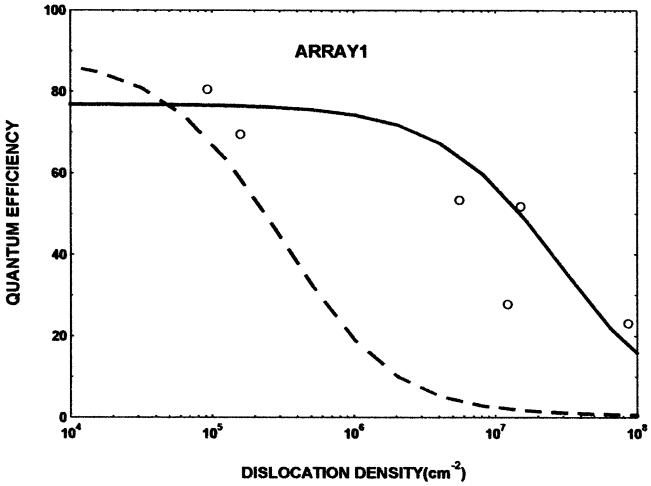

Fig. 6. Effect of dislocations on quantum efficiency (8.3 μm) at 77 K in array1. Continuous and broken line curves are, respectively, the calculated curves using the present model and the model used in [3] while points are the experimental data from [3].

B. Quantum Efficiency and Spectral Response

A comparison of the quantum efficiency calculated from the combination of (15) and (19) with the experimental data is shown in Figs. 6 and 7. For the sake of comparison, broken line curve in each of these figures show the calculated quantum efficiency using the following relation to estimate the effective diffusion length of minority carriers.

$$\frac{1}{L_{\text{eff}}^2} = \frac{1}{L_0^2} + \frac{\pi^3 N}{4}. \tag{20}$$

This relation is sometimes referred to as effective diffusion length model, has been used in GaAs and HgCdTe by several authors [3], [4], [10]–[12]. It can be clearly observed from Figs. 6 and 7 that the effective diffusion length of minority

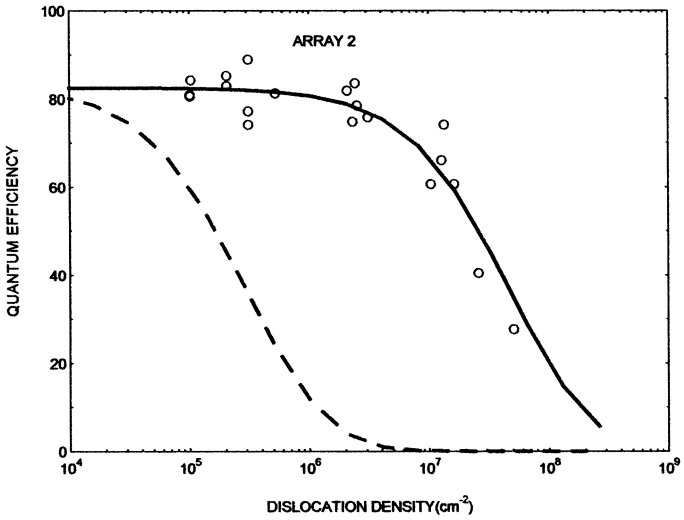

Fig. 7. Effect of dislocations on quantum efficiency (4.0 μm) at 77 K in array2. Continuous and broken line curves are, respectively, the calculated curves using the present model and the model used in [3] while points are the experimental data from [3].

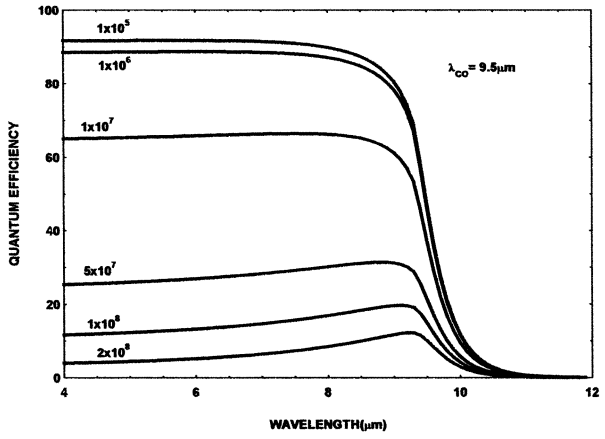

(a)

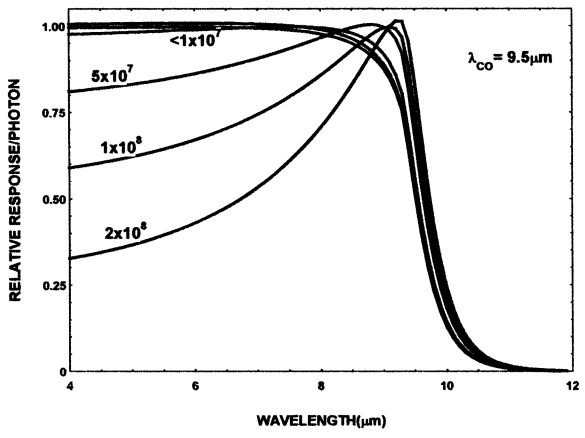

(b)

Fig. 8. (a) Calculated quantum efficiency and (b) corresponding relative spectral response at 77 K as a function of dislocation density (marked on each curve) for diodes with 9.5-μm cutoff wavelength.

carriers calculated from the present model (19) provide an excellent fit to the experimental data than obtained by using (20). In addition we have also shown in Fig. 8(a) and (b) the calculated quantum efficiency and relative spectral response,

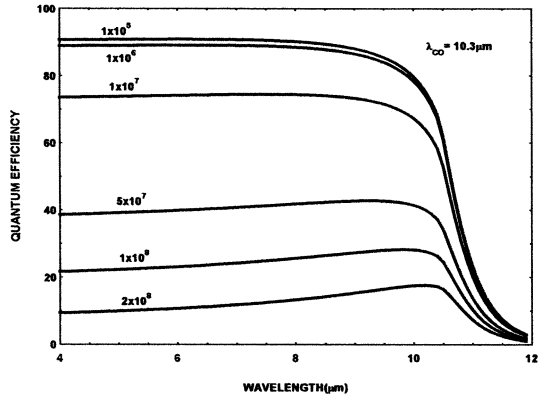

(a)

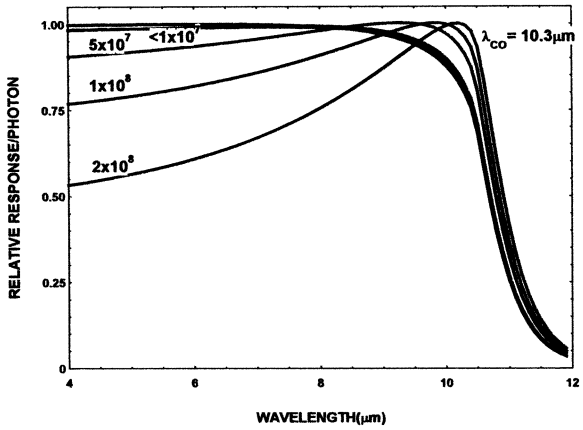

(b)

Fig. 9. (a) Calculated quantum efficiency and (b) corresponding relative spectral response at 77 K as a function of dislocation density (marked on each curve) for diodes with 10.3-μm cutoff wavelength.

respectively, for different values of dislocation density in the base material for array 1. Similar curves for array 2 are shown in Fig. 9(a) and (b). It is clearly visible from Fig. 8(a) and (b) that the quantum efficiency decreases over the entire wavelength range with the increase in dislocation density. The enhancement of relative spectral response per photon [seen in Figs. 8(b) and 9(b)] near the cutoff wavelengths of the two arrays with the increasing dislocation density is simply an artefact of normalization of the curves shown in Figs. 8(a) and 9(a) with respect to the peak response. The Figs. 8(b) and 9(b) have been, however, shown here to emphasize the excellent agreement of our model with the experimental data of Johnson *et al.* [3]. The large reduction in the relative spectral response/quantum efficiency at short wavelengths [Figs. 8(a), (b), 9(a) and (b)] is quite expected since in a backside-illuminated diode most of the absorption takes place near the epi-substrate interface, i.e., away from the junction. Thus a reduction in the effective diffusion length of the carriers with increasing dislocation density causes more and more degradation at shorter wavelengths. On the other hand, at longer wavelengths, most of the incident radiation is absorbed near the junction and thus a change in effective diffusion length does not significantly affect the relative spectral response/quantum efficiency.

IV. Summary

In this paper, a simple analytical model to calculate the impedance (shunt) of individual line dislocations along the thickness of the wafer has been proposed. The model is essentially based on the calculation of the recombination velocity of the carriers at the dislocations. Assuming the dislocations to be uniformly distributed all over the sample, temperature and dislocation dependence of R_0A product, quantum efficiency and spectral response could be satisfactorily modeled in case of LWIR HgCdTe photodiodes below dislocation density of 10^7 cm^{-2}. The large scatter of the experimental data in the high dislocation density region has been interpreted as an indication of the variations in the size of the dislocations due to the variations in the number of dislocations merging together or clustering of dislocations at different sites.

Acknowledgment

The authors are thankful to Prof. V. Kumar, Director, Solid State Physics Laboratory, Delhi, for the encouragement and his kind permission to publish this paper.

References

[1] S. M. Johnson, M. H. Kalisher, W. L. Ahlgren, J. B. James, and C. A. Cockrum, "HgCdTe 128 × 128 infrared focal plane arrays on alternative substrates of CdZnTe/GaAs/Si," *Appl. Phys. Lett.*, vol. 56, pp. 946–948, Mar. 1990.

[2] J. B. Varesi, R. E. Bornfreund, A. C. Childs, W. A. Radford, K. D. Maranowski, J. M. Peterson, S. M. Johnson, L. M. Giegerich, T. J. De Lyon, and J. E. Jensen, "Fabrication of high-performance large format MWIR focal plane arrays from MBE grown HgCdTe on 4," *Silicon Substrates, J. Electron. Mater.*, vol. 30, pp. 566–573, 2001.

[3] S. M. Johnson, D. R. Rhiger, J. P. Rosebeck, J. M. Peterson, S. M. Taylor, and M. E. Boyd, "Effect of dislocations on the electrical and optical properties of long-wavelength infrared HgCdTe photovoltaic detectors," *J. Vac. Sci. Technol. B*, vol. 10, no. 4, pp. 1499–1506, July/Aug. 1992.

[4] K. Jowikowski and A. Rogalski, "Effect of dislocations on performance of LWIR HgCdTe photodiodes," *J. Electron. Mater.*, vol. 29, pp. 736–741, 2000.

[5] A. Many, Y. Goldstein, and N. B. Grover, *Semiconductor Surfaces*. Amsterdam, The Netherlands: North-Holland, 1965, p. 197.

[6] M. B. Riene, A. K. Sood, and T. J. Tredwell, *Photovoltaic Infrared Detectors*, R. K. Willardson and A. C. Beer, Eds. New York: Academic, 1981, p. 201.

[7] V. Gopal, S. K. Singh, and R. M. Mehra, "Analysis of dark current contributions in mercury cadmium telluride junction diodes," *Infrared Phys. Technol.*, vol. 43, no. 6, pp. 317–326, 2002.

[8] V. Gopal, S. Gupta, R. K. Bhan, R. Pal, P. K. Chaudhary, and V. Kumar, "Modeling of dark characteristics of mercury cadmium telluride n^+-p junctions," *Infrared Phys. Technol.*, vol. 44, no. 2, pp. 143–152, 2003.

[9] J. P. Rosebeck, R. E. Starr, S. L. Price, and K. J. Riley, "Background and temperature dependent current-voltage characteristics of HgCdTe photodiodes," *J. Appl. Phys.*, vol. 53, no. 9, pp. 6430–6440, Sept. 1982.

[10] M. Yamaguchi and C. Amano, "Efficiency calculations of thin-film GaAs solar cells on Si substrates," *J. Appl. Phys.*, vol. 45, pp. 3601–3606, 1985.

[11] M. Yamaguchi, A. Yamamoto, and Y. Itoh, "Effect of dislocations on the efficiency of thin-film GaAs solar cells on Si substrates," *J. Appl. Phys.*, vol. 59, pp. 1751–1753, 1986.

[12] J. C. Zolper and A. M. Barnett, "The effect of dislocations on the open-circuit voltage of gallium arsenide solar cells," *IEEE Trans. Electron Devices*, vol. 37, pp. 478–484, Feb. 1990.

[13] A. Rogalski, "Mercury cadmium telluride photodiodes at the beginning of the next millennium," *Defence Sci. J.*, vol. 51, pp. 5–34, Jan. 2001.

[14] S. P. Tobin, M. H. Weiler, M. A. Hutchins, T. Parodos, and P. W. Norton, "Advances in composition control for 16 μM LPE P-on-n HgCdTe heterojunction photodiodes for remote sensing applications at 60 K," *J. Electron. Mater.*, vol. 28, pp. 596–602, 1999.

[15] J. Yoshino, J. Morimoto, H. Wada, A. Ajisawa, M. Kawano, and N. Oda, "Studies of relationship between deep levels and R_0A product in mesa type HgCdTe devices," *Opto-Electron. Rev.*, vol. 7, pp. 361–367, 1999.

[16] P. Capper, *Properties of Narrow Gap Cadmium Based Compounds*, ser. 10, P. Capper, Ed., 1991, Inspec, IEELondon, UK, p. 41.

[17] G. L. Hansen, J. L. Schmit, and T. N. Casselman, "Energy gap versus alloy composition and temperature in $Hg_{1-X}Cd_XTe$," *J. Appl. Phys.*, vol. 53, pp. 7099–7101, 1982.

[18] G. L. Hansen and J. L. Schmit, "Calculation of intrinsic carrier concentration in $Hg_{1-X}Cd_XTe$," *J. Appl. Phys.*, vol. 54, pp. 1639–1640, 1983.

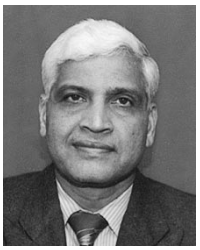

Vishnu Gopal received the M.Sc. degree in physics from Agra University, Agra, India, in 1965 and the Ph.D. degree, also in physics, from Meerut University, Meerut, India, in 1984.

His research interests include the optical and electrical characterization of semiconductor materials, ion implantation studies in semiconductors, IR detectors, and focal plane arrays. He is the author or coauthor of 107 research papers published in refereed international journals and presented/published in the Proceedings of national and international conferences. He joined Solid State Physics Laboratory, Delhi, India, in 1967 and is currently guiding the activity on the development of IR detectors in the laboratory as Associate Director.

Dr. Gopal is listed in Marquis' International *Who's Who in the World*.

Sudha Gupta received the M.Sc. degree in physics in 1986 from the University of Delhi, Delhi, India.

She joined Solid State Physics Laboratory, Delhi, in 1987 and is currently with the IR division working on the development of IR detectors and focal plane arrays.